Computers in Biology and Medicine 113 (2019) 103419

Contents lists available at ScienceDirect

Computers in Biology and Medicine

journal homepage: http://www.elsevier.com/locate/compbiomed

Infrared (IR) thermography as a potential screening modality for carotid artery stenosis

Ashish Saxena[a], E.Y.K. Ng[a,*], Soo Teik Lim[b]

[a] School of Mechanical and Aerospace Engineering, Nanyang Technological University, 50 Nanyang Ave, 639798, Singapore
[b] Department of Cardiology, National Heart Center Singapore, 5 Hospital Dr, 169609, Singapore

ARTICLE INFO

Keywords:
Carotid artery stenosis
Atherosclerosis
Infrared (IR) thermography
Binary classification
Support vector machine (SVM)
Cardiovascular imaging

ABSTRACT

In the present study, an infrared (IR) thermal camera was used to map the temperature of the target skin surface, and the resulting thermal image was evaluated for the presence of carotid artery stenosis (CAS). In the presence of stenosis in the carotid artery, abnormal temperature maps are expected to occur on the external skin surface, which could be captured and quantified using IR thermography. A Duplex Ultrasound (DUS) examination was used to establish the ground truth. In each patient, the background-subtracted thermal image, referred to as *full thermal image*, was used to extract novel parametric *cold thermal feature images*. From these images, statistical features, viz., correlation, energy, homogeneity, contrast, entropy, mean, standard deviation (SD), skewness, and kurtosis, were calculated and the two groups of patients (control and diseased: a total of 80 carotid artery samples) were classified. Both cut-off value- and support vector machine (SVM)-based binary classification models were tested. While the cut-off value classification model resulted in a moderate performance (70% accurate), SVM was found to have classified the patients with high accuracy (92% or higher). This preliminary study suggests the potential of IR thermography as a possible screening tool for CAS patients.

1. Introduction

Carotid artery stenosis (CAS) or atherosclerosis, wherein narrowing of the carotid artery passage occurs as a result of endothelial cell dysfunction and inflammation that leads to thrombosis formation [1], is of great interest to the scientific medical imaging and clinical communities across the globe. A complete choke (occlusion) of the internal carotid artery (ICA: supply blood to the brain) or dislodging of the atherosclerosis tissue to the brain affects the normal brain functioning and may cause irreversible damage to the brain tissue or leads to debilitating stroke [2]. According to the American Heart Association (AHA) [3], in the United States alone, around 795,000 cases of stroke are reported yearly, and on average, every 4 min, someone dies of a stroke. Therefore, screening, imaging, diagnosis, and monitoring of CAS play an essential role in the clinical decision making and overall CAS treatment profile. In the clinical settings, imaging modalities like Computed Tomography Angiography (CTA), Magnetic Resonance Angiography (MRA), and Duplex Ultrasound (DUS) are mainly used to manage the CAS related cases [4,5]. DUS is the most widely available, low cost, and low-risk CAS imaging modality; however, it needs trained personnel to perform and interpret the examination and suffers from inter/intra-observer variability [6]. While CTA has risk associated with X-ray radiation exposure, MRA is not suitable for patients with certain types of implants, viz. cochlear (ear) implants, clips used for brain aneurysms, metal coils placed within blood vessels, older cardiac defibrillators and pacemakers, etc., because of magnetic fields involved [7–9]. In both the modalities (CTA and MRA), contrast usage may lead to adverse allergic reactions or nephropathy [10]. While both CTA and MRA machines need a large area for installation, MRA is a time-consuming procedure, costly, and not readily available [11]. Therefore, a reliable, non-invasive, cost-effective, automated, fast, and easy-to-use alternate CAS screening tool will complement the current clinical CAS imaging and treatment profile.

It is evident that the occurrence of CAS causes thermal changes, such that the presence of stenosis affects the blood flow (turbulent flow across the lesion) in the carotid artery [12]; alters the heat transfer to the surrounding tissue and the resultant outer skin surface temperature [13–15]. In the past, contact-based temperature measurement, called plate thermography, was used to correlate the presence of abnormal temperature map with CAS. Plate thermography, wherein a flexible foil, coated with specific cholesterol ester, changes color due to temperature oscillations, was used to map the forehead temperature in 300 patients;

* Corresponding author.
E-mail address: MYKNG@ntu.edu.sg (E.Y.K. Ng).

https://doi.org/10.1016/j.compbiomed.2019.103419
Received 31 July 2019; Received in revised form 27 August 2019; Accepted 27 August 2019
Available online 28 August 2019

the method showed positive results (abnormality) in 39 patients against 34 patients using Doppler sonography [16]. Thereafter, a non-contact facial temperature measurement, using an infrared (IR) thermal camera [17–19], that correlates to the presence of CAS was performed by Capistrant and Gumnit [20]. Of the 30 patients, suffering from angiographically proven carotid stenosis or occlusion, an abnormal thermal map was observed in 57% of the cases. Monitoring the temperature variation among the geometrically symmetrical locations of the human body (ocular, limbs, etc.) could prove to be an indirect cardiovascular disease detection marker [21]. With reference to CAS detection, one such correlation was studied by Morgan et al. [22], on 24 patients, wherein the ocular temperature was correlated ($r = -0.67$) to the degree of stenosis in the carotid artery. Therefore, temperature measurement, especially using IR thermography, could fulfill the need of a desirable CAS screening modality. In the last two decades, however, despite the development of sophisticated image processing, object detection, machine learning, and deep learning algorithms, no IR thermography-based, highly accurate and clinically proven, CAS detection method has been reported in the field.

Unlike the previous IR thermography-based CAS detection studies [21,22], wherein the original thermal image and its mean temperature were used to classify the two groups of patients (control and diseased), in the present study, using the original *full thermal image*, a novel parametric *cold thermal feature image* extraction method is proposed. Moreover, in the past, the target area of thermal scan in such studies was either the temporal (forehead) or the ocular (eyes) region. The proposed method is taking the IR thermal scan from either side of the neck, including the face region. The *full thermal image* and the extracted parametric *cold thermal feature images* were quantitatively analyzed with the help of statistical features, viz., correlation, energy, homogeneity, contrast, entropy, mean, standard deviation (SD), skewness, and kurtosis. While previous studies were limited to cut-off value-based binary classification model, in the present study, additionally, support vector machine (SVM)-based binary classification model was applied on the statistically significant features, and the respective classification performance is reported.

2. Materials and methods

2.1. Study population

In this prospective study, 40 patients (38 males and 2 females), in the age group of 45–71 years old (mean = 61.85 years and SD = 6.78 years), were recruited under the clinical research study approved by Centralized Institutional Review Board (CIRB Ref No.: 2017/2119), SingHealth, Singapore. The patients were recruited at the Vascular Lab of National Heart Center Singapore (NHCS). Patients with a clinical indication for carotid DUS for arterial stenosis detection, as identified by the physicians at NHCS, were approached to participate in the study. Patients with previously known significant stenosis in the subclavian artery or multiple stenoses or occlusion in cerebral circulation were excluded from the study.

2.2. Duplex ultrasound examination

Upon signing the informed consent form, the patients undergo the standard carotid DUS examination performed by the trained sonographer at NHCS. The stenosis grading, in the Common Carotid Artery (CCA), Internal Carotid Artery (ICA), and External Carotid Artery (ECA), was done using a combined morphological (diameter) and hemodynamic (peak systolic and end-diastolic velocities) criterion [23] as per the standard grading protocol followed at the Vascular Lab, NHCS. Studying the carotid artery on each side of the neck as an individual sample, this study utilized a total of N = 80 samples. Based on the outcome of the DUS examination, the left and right carotid arteries of the patients were labeled with the stenosis grading (either in the CCA, ICA or ECA region of the carotid artery), and hence, the study samples were divided into 4 subgroups, namely, one Control group as 0% (C) stenosis and three Diseased groups with 10%–29% (D1), 30%–49% (D2), and ≥50% (D3) stenosis, as shown in Fig. 1. Derived from these four groups, two more groups, namely, extended control (C': 0%–29% stenosis) and extended diseased (D': ≥30% stenosis) groups, were also made.

2.3. Infrared (IR) thermography examination

Following the Duplex Ultrasound examination, the patients were prepared for the IR thermography examination on the same day. As a part of standard medical thermography protocol, the patients were asked to rest for 15 min in a temperature-controlled room maintained at $23 \pm 0.5\,^{\circ}$C temperature and 50% relative humidity [24]. A passive thermal scan (with no external stimulation), on either side of the neck and face region, was taken using VarioCAM IR thermal camera by InfraTec. The IR thermal camera, equipped with an uncooled microbolometer detector, produces a 2-dimensional (2-D) thermal images (rows x columns: 240 × 320 pixels) with a temperature resolution of less than 0.1 °C. Evident from the studies on neck temperature-based pulse measurement [25,26], the cardiac cyclic nature (systolic and diastolic) of the blood flow in the carotid artery results in a local and infinitesimally small change in the skin temperature with no effect on the global temperature maps, a passive image taken at any instant of the cardiac cycle can be used in the present analysis.

2.4. Parametric cold thermal feature image extraction

The original thermal image, taken on either side of the neck, has neck, face, head, cloth, and background details, as shown in Fig. 2. For image noise and background subtraction, the original thermal image, after converting into a grayscale normalized image with intensity value in the range of 0–1, was first passed through a 2-D median filter. The resultant image was then used to calculate a global threshold value using Otsu's method [27,28]. The threshold value was calculated as such it minimizes the intraclass variance of the pixels in the image. Using this threshold value, a mask image was created. Masking the original thermal image with the mask image resulted in a background-subtracted image (Fig. 2). Given the temperature of the clothing, on the patient's body, is higher than the background (surrounding) but lower than the skin temperature, if, at all visible in the original thermal image, it was not masked out entirely in the background-subtracted image. Hence, manual segmentation was performed to remove the clothing part from the image; resulting in a cloth segmented *full thermal image* (Fig. 2). From the *full thermal image*, *cold thermal feature images* were extracted using a parametric threshold temperature method given by Equation (1). For a given *full thermal image,* since the threshold value is derived below the mean temperature, at a specific k parameter value, the resultant image is referred to as a *cold thermal feature image* (Fig. 2).

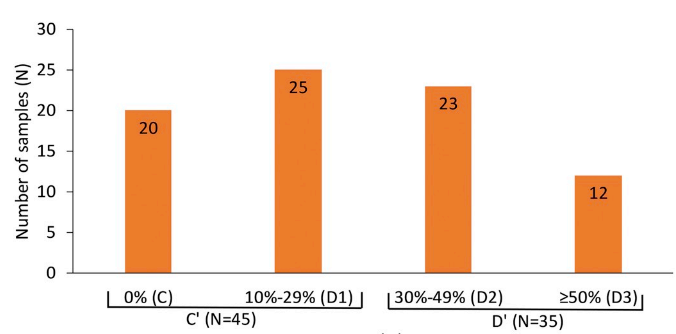

Fig. 1. Carotid sample distribution based on stenosis grading by Duplex Ultrasound.

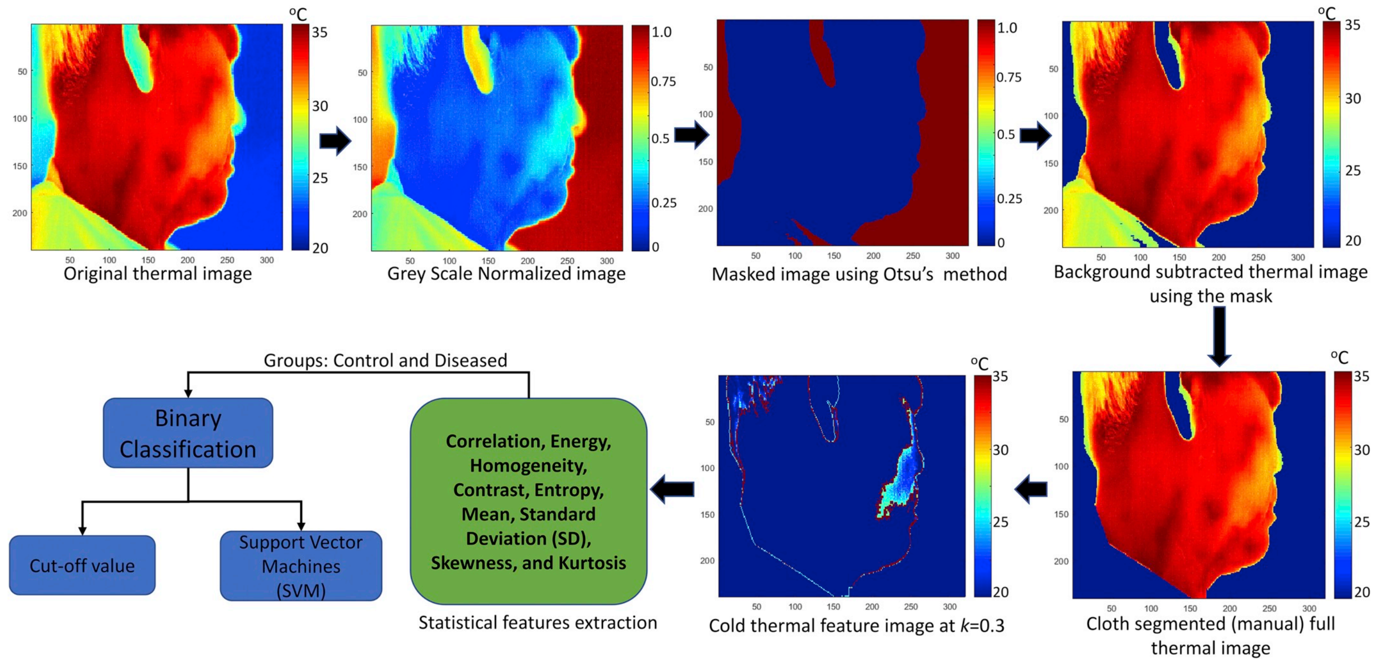

Fig. 2. Thermal image processing: normalizing, masking, segmentation, feature extraction, and classification.

$$T_{ck} = T_m - k(T_m - T_{mi}) \tag{1}$$

where, T_{ck} is the cold thermal feature threshold temperature (^{o}C) at the defined k parameter that varies from 0.1 to 0.9 in a step size of 0.1. T_{mi} and T_m are the minimum and mean temperature (^{o}C) value calculated from all the non-zero pixels in the given *full thermal image*, respectively. For the given k value, all the image pixels with temperature value more than T_{ck} were replaced with zero (Fig. 2). This resulted in a series of nine (for $k = 0.1$ to 0.9) *cold thermal feature images*.

Unlike the case of tumor, cervical lymph node metastasis, internal injury, etc. [29], where the presence of pathological condition is defined by a high-temperature region in the thermal image, in the present study, a region of lower temperature is expected to be the indication of stenosis in the carotid artery [20]. In the presence of stenosis, changes in the hemodynamics of the carotid artery take place. This results in a lower rate of heat transfer to the external skin tissue surface and hence appears as a low-temperature region in the resultant thermal image [15]. To quantitatively compare the temperature distribution in the thermal image, between the normal and stenosis cases, statistical features were used. In all the thermal scans, from each of the *full thermal image* and its corresponding nine *cold thermal feature* images, nine statistical features, viz., correlation, energy, homogeneity, contrast, entropy, mean, standard deviation (SD), skewness, and kurtosis, were calculated (Fig. 2) [30].

2.5. Binary classification

Using the significant statistical features, classification of the two groups of patients (control and diseased) was done using the cut-off value and Support Vector Machine (SVM)-based classification models (Fig. 2). For both the classification models, the performance was evaluated with the standard definition (refer supplementary material: S1 Equations (1s) to (5s)) of sensitivity, specificity, accuracy, positive predictive value (PPV), and negative predictive value (NPV).

2.5.1. Cut-off value-based classification

For each of the extracted significant statistical feature, from each of the nine *cold thermal feature images*, a cut-off value was used to classify the two groups of patients (control and diseased). The optimum cut-off value was defined using the receiver operating curve (ROC) analysis, which is widely used for binary classification problems in medical diagnosis applications [31,32]. In the ROC analysis, at a given cut-off value, the *sensitivity* of the classification is plotted against the (1 − *specificity*). For a given set of feature values, from the two groups of patients (control and diseased), several cut-off values are tested and the optimal cut-off value point, from where the distance to the point of ($sensitivity = 1,\ 1 - specificity = 0$) is minimum [33], is chosen from the ROC curve. The classification sensitivity and specificity are highest at this optimal point. Additionally, the area under the ROC curve (AUC) provides a quantitative measure of classification success: 0.5 is poor, while 1 is the best classification model.

2.5.2. Support vector machine (SVM)-based classification

In the present study, Support Vector Machine (SVM)-based machine learning classification was used. SVM is widely applied for medical thermography-based disease diagnosis applications such as breast cancer [34,35], cervical lymph node metastasis [24], knee osteoarthritis [36], etc. In SVM, for a given set of feature data from the two group of patients (control and diseased), a hyperplane is introduced such that the closest feature data points in the two classes (called as support vectors), on either side of the hyperplane, are well separated from each other. The objective is to select an optimal hyperplane that maximizes the distance between the hyperplane and the support vectors [37]. Where the feature data set is not linearly separable, a non-linear SVM model is used. In non-linear SVM, the features are mapped into a higher feature space (called *Kernel mapping*), from where a linear hyperplane separation is possible [38]. In the present study, non-linear (RBF: radial basis function) SVM model was tested (refer supplementary material: S2). To entirely utilize the available data, a seven-fold cross-validation SVM model was used [39]. In this model, from the total available samples, using all the statistically significant features from the *full* and *cold thermal feature images* (Table 1), the samples were randomly divided into seven subsets. At a time, one subset was used for the training while the remaining ones were used for the testing. This process was repeated seven times to ensure the usage of each of the subsets for both training and testing purpose. To ensure a random mix of the data, in the present study, the cross-validation model was iterated ten times. At each iteration, of the generated seven training models, the one with the highest

Table 1
List of significant features ($p < 0.05$) in various groups of patients.

k	Features	Feature average value (±95% CI)								
		Group (C′ and D′)			Group (C and D1)			Group (D2 and D3)		
		C' (N = 45)	D' (N = 35)	*p*-value	C (N = 20)	D1 (N = 25)	*p*-value	D2 (N = 23)	D3 (N = 12)	*p*-value
Full thermal image	Energy	0.53 ± 0.01	0.51 ± 0.01	0.036	NA	NA	NA	NA	NA	NA
	Mean	32.77 ± 0.13	32.48 ± 0.18	0.006	32.90 ± 0.21	32.67 ± 0.16	0.042	NA	NA	NA
	Skewness	−0.48 ± 0.12	−0.25 ± 0.12	0.004	−0.64 ± 0.15	−0.36 ± 0.16	0.008	−0.31 ± 0.15	−0.10 ± 0.15	0.029
	Kurtosis	3.44 ± 0.28	2.97 ± 0.28	0.011	NA	NA	NA	NA	NA	NA
0.1	Mean	31.79 ± 0.10	31.57 ± 0.17	0.017	NA	NA	NA	NA	NA	NA
	SD	0.59 ± 0.04	0.52 ± 0.04	0.010	0.63 ± 0.06	0.55 ± 0.05	0.040	NA	NA	NA
0.2	Homogeneity	NA	NA	NA	0.973 ± 0.004	0.968 ± 0.003	0.028	NA	NA	NA
	Contrast	NA	NA	NA	1.52 ± 0.21	1.81 ± 0.19	0.028	NA	NA	NA
	Entropy	0.57 ± 0.04	0.61 ± 0.04	0.044	NA	NA	NA	NA	NA	NA
	Mean	31.54 ± 0.09	31.37 ± 0.15	0.030	NA	NA	NA	NA	NA	NA
	SD	0.55 ± 0.04	0.48 ± 0.03	0.008	0.58 ± 0.05	0.52 ± 0.05	0.039	NA	NA	NA
0.3	Energy	0.80 ± 0.02	0.77 ± 0.03	0.032	NA	NA	NA	NA	NA	NA
	Homogeneity	NA	NA	NA	0.979 ± 0.003	0.973 ± 0.004	0.022	0.974 ± 0.004	0.968 ± 0.005	0.035
	Contrast	NA	NA	NA	1.21 ± 0.15	1.50 ± 0.23	0.022	1.45 ± 0.21	1.77 ± 0.26	0.035
	Entropy	0.44 ± 0.04	0.50 ± 0.05	0.033	NA	NA	NA	NA	NA	NA
	SD	0.49 ± 0.03	0.44 ± 0.03	0.013	0.52 ± 0.05	0.47 ± 0.04	0.043	NA	NA	NA
0.4	Energy	0.85 ± 0.02	0.83 ± 0.03	0.042	NA	NA	NA	NA	NA	NA
	SD	0.43 ± 0.03	0.39 ± 0.03	0.028	0.46 ± 0.04	0.41 ± 0.03	0.032	NA	NA	NA
0.5	SD	0.38 ± 0.02	0.34 ± 0.02	0.008	0.40 ± 0.03	0.36 ± 0.02	0.038	NA	NA	NA
0.6	SD	0.31 ± 0.02	0.28 ± 0.02	0.004	NA	NA	NA	NA	NA	NA
0.7	SD	0.24 ± 0.01	0.21 ± 0.01	0.003	NA	NA	NA	NA	NA	NA
0.8	SD	0.16 ± 0.01	0.14 ± 0.01	0.0005	0.169 ± 0.012	0.155 ± 0.009	0.040	NA	NA	NA
	Kurtosis	NA	NA	NA	NA	NA	NA	1.97 ± 0.11	1.83 ± 0.05	0.011
0.9	SD	0.08 ± 0.004	0.07 ± 0.01	0.002	0.086 ± 0.006	0.079 ± 0.005	0.032	NA	NA	NA
	Skewness	NA	NA	NA	−0.02 ± 0.06	−0.10 ± 0.05	0.025	−0.16 ± 0.06	−0.03 ± 0.06	0.003

C: 0% stenosis; D1: 10%–29% stenosis; D2: 30%–49% stenosis; D3: ≥50% stenosis; C': 0%–29% stenosis; D': ≥30% stenosis; NA: Not Applicable (for non-significant features with $p \geq 0.05$).

classification error was used to report the classification performance [40]. At the end of the ten iterations, the average values (±confidence interval) of the performance parameters, viz. sensitivity, specificity, accuracy, PPV, and NPV, were reported.

2.5.3. *Classification strategy*

In clinical settings, accurately screening patients with 30% or more stenosis (vulnerable/unstable: more likely to rupture) is of more importance than less than 30% stenosis [41], such that the false-positive cases are affordable over the false negative ones. To evaluate the classification performance in such a case, in the present study, extended groups C′ and D′ were classified first, and then a sub-classification of groups C′ and D' into the group (C and D1) and (D2 and D3), respectively, was performed (Fig. 3).

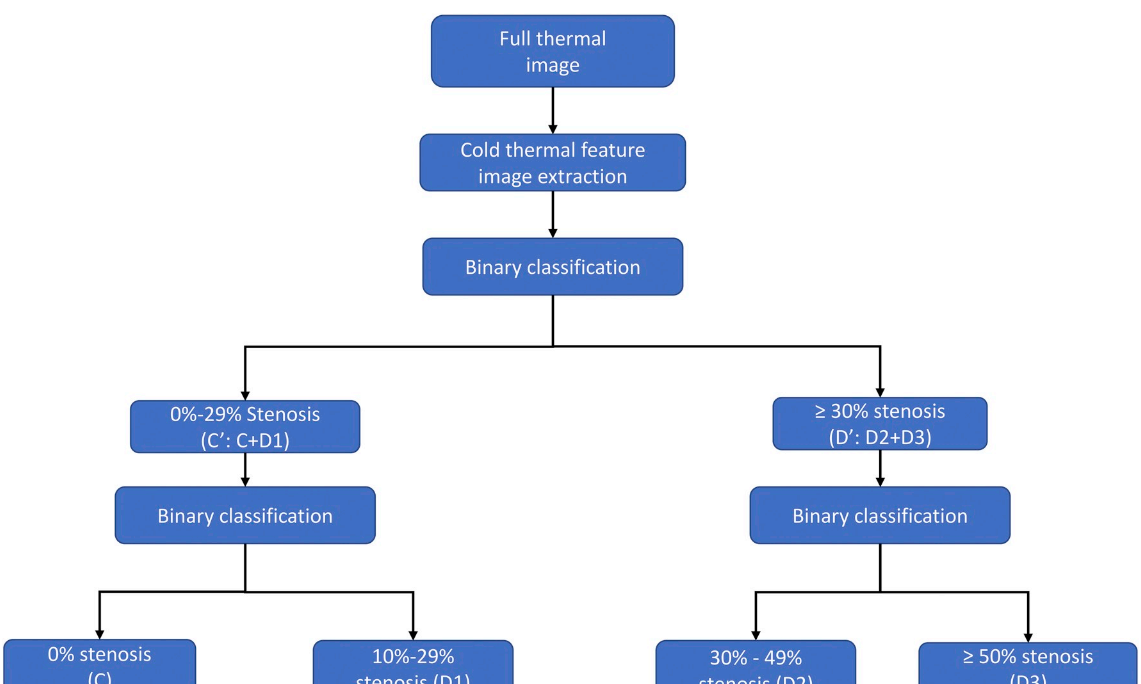

Fig. 3. Binary classification flow chart for control (C: 0% stenosis), diseased (D1: 10%–29% stenosis; D2: 30%–49% stenosis; D3: ≥50% stenosis; and D: ≥ 10% stenosis), extended control and diseased (C': 0%–29% stenosis; D': ≥30% stenosis) groups of patients.

2.6. Data analysis

Extraction of the *cold thermal feature images* from the original *full thermal images*, statistical feature calculation, evaluation of statistically significant features, followed by the classification of patients using cut-off value and SVM-based classification models, (Fig. 2), the processing was done in MATLAB toolbox (academic license version: R2017B) by MathWorks. To determine the statistical significance of the difference in the target skin surface temperature and the calculated statistical features for the *full* and *cold feature thermal images*, between the two groups of patients (control and diseased), student's *t*-test, with a significance level of 0.05 (*p*-value), was used. Shapiro-Wilk test [42] was used to test the data normality. Non-parametric Mann-Whitney *U* test was applied [43] for data failing normality test. Average values, of any of the measured or calculated quantities, are reported with 95% confidence interval (95% CI).

3. Results

Fig. 4 shows the ultrasound images of the internal carotid artery (ICA), in a single patient from each of the four groups of patients, namely, C, D1, D2, and D3 (Fig. 1), in the increasing order of stenosis degree. Adjacent to the ultrasound images, in Fig. 4, the *full thermal images* are shown. With a qualitative visual inspection, it can be observed that the overall temperature distribution changes from group C to D3. In each patient, using Equation (1), nine *cold thermal feature images* were extracted at parametric k values ranging from 0.1 to 0.9. Corresponding to the *full thermal image*, Fig. 5 shows the *cold thermal feature image*, for a single patient in each group, at $k = 0.1$, 0.4, and 0.7. As the k value increases, the region of thermal feature diminishes, while for the same k value, the thermal feature becomes more prominent as the stenosis degree increases from group C to D3.

In each patient, from the *full thermal image* and its nine sub-images (*cold thermal feature images* at $k = 0.1$ to 0.9), statistical features, viz. correlation, energy, homogeneity, contrast, entropy, mean, standard deviation (SD), skewness, and kurtosis, were extracted. Based on the classification strategy, in Fig. 3, feature statistical significance ($p < 0.05$), between the classification groups (C′ and D'), (C and D1), and (D2 and D3), was evaluated and summarized in Table 1.

Considering each of the significantly different statistical features, extracted from the *full thermal image*, the performance of cut-off value based binary classification is summarized in Table 2. Among the three classification groups, skewness was found to be the only common significant feature that provides the highest classification accuracy. Moving on, the significantly different statistical features, extracted from the *cold thermal feature images*, were used to perform the cut-off value-based classification (refer supplementary material: Tables S1 and S2). For the classification group (C′ and D'), of all the statistical features among *cold thermal feature images*, standard deviation (SD) was found to be the only significantly different feature at all the values of k (Table 1 and Fig. 6a).

Choosing the best performance feature, Table 3 summarizes the results of cut-off value-based classification and Fig. 6b shows its corresponding ROC curve. While the group (C′ and D') was found to have best classified using the *full thermal image* itself, use of *cold thermal feature images*, at $k = 0.2$ and 0.9, was found to have performed better for the sub-classification of groups (C and D1) and (D2 and D3). Even though the features are significantly different, the performance of the cut-off value-based classification was found to be poor; therefore, in the present study, the SVM-RBF model was applied to perform the classification. Using all the significant features (Table 1) from the *full thermal image* and its sub-images (*cold thermal feature images*), Table 4 summarizes the outcome of the SVM classification.

4. Discussion

As per clinical DUS evaluation, using both the B-mode and color doppler 2-D ultrasound images, the original and the reduced (due to stenosis) blood vessel diameter boundaries were marked (Fig. 4). While the peak systolic blood flow velocity in these single patients, from group C, D1, D2, and D3, was found to be 71, 55, 60, and 33 cm/s, respectively, the end-diastolic blood flow velocity was found to be 21, 13, 17, and 4 cm/s, respectively. The average (±95% CI) peak systolic velocities, in group C, D1, D2, and D3, were 61.1 ± 8.5, 57.8 ± 4.7, 67.7 ± 11.3, and 117 ± 53.5 cm/s, respectively, and the average end-diastolic velocities were 22.5 ± 3, 20.9 ± 2.2, 23.4 ± 4.3, and 39.3 ± 21.7 cm/s, respectively. Given the group D3 has a wide range of stenosis degree cases (from 50% to near occlusion) and presence of multiple location stenosis in the CCA, ICA, and ECA region, it resulted in a high 95% CI velocity value. With the reduction in the diameter, from group C to D3, the blood flow velocity tends to increase, which is accompanied by the formation of recirculation zone past the stenosis and reduction in the adequate blood volumetric flow [44–46]. This affects the surrounding tissue heat transfer, which is expected to result in variational temperature features on the outer skin surface [5,15]. To quantify this temperature change, in the present study, thermal images were used and the classification performance, among the groups of control and diseased patients, was evaluated as illustrated in Fig. 3.

In Fig. 4, while for the group C patient, the temperature distribution is observed to be more uniform within high-temperature zones (31 °C–34 °C), for group D1 to D3, as a result of presence of stenosis in the carotid artery, the temperature distribution resulted into cold temperature zones (29 °C–32 °C). The mean (±95% CI) temperatures, in group C, D1, D2, and D3, were found to be 32.90 ± 0.21, 32.67 ± 0.16, 32.52 ± 0.23, and 32.39 ± 0.27, respectively; mean temperature decreases with the increase in degree of stenosis in the carotid artery [22]. As per the proposed classification strategy (Fig. 3), the mean temperature in extended classification group (C′ and D′) was found to be significantly higher for group C' (C': 32.77 ± 0.13 versus D': 32.48 ± 0.18, $p = 0.006$). For the sub-classification groups (Table 1), while the mean temperature was significantly different in (C and D1), it was insignificant in the group (D2 and D3). Therefore, in addition to the mean temperature feature, more statistical features were extracted from the *full thermal images*. In the classification group (C′ and D′), Energy, Skewness, and Kurtosis features were also found significantly different. Moreover, while in the classification group (C and D1), Skewness feature was also found significant, in the classification group (D2 and D3), only Skewness was found significant (Table 1). Using these significant features, the cut-off value-based classification of groups (C′ and D'), (C and D1), and (D2 and D3) yielded the highest accuracy of 69%, 64%, and 70%, respectively, for the Skewness feature (Table 2). Using the Skewness feature, in the present study, the sensitivity of classifying the patients with ≥50% stenosis (group D3), using cut-off value-based binary classification model, was found to be 80%, which is around 40% and 864% better than the one achieved using mean temperature in the work of Capistrant and Gumnit (57%) [20] and Morgan et al. (8.3%) [22], respectively (Fig. 7).

To further enhance this classification, in the present study, the proposed *cold thermal feature image* extraction method was applied (Equation (1)). For the classification group (C′ and D'), at all the k values, though SD feature was found to be significantly different (Table 1), except at $k = 0.4$, the feature value overlap, between the two groups of patients, was found to have decreased with the increase in k value. This is further corroborated from the AUC curve that shows an increasing trend (linear regression, $R^2 = 0.68$) with the k value increment (Fig. 6a). A lower R^2 value is the result of the catastrophic change in the AUC value at $k = 0.4$ and 0.8. While at $k = 0.4$, the lower AUC is the result of the high overlap in the feature values that resulted in a high p-value of 0.028, at $k = 0.8$, a high value of AUC is the result of the low overlap in the feature values that resulted in a lower p-value of 0.0005 (Table 1). Corresponding to these AUC values, at $k = 0.1$ to 0.9, the classification model performance, in terms of sensitivity and specificity, can be found

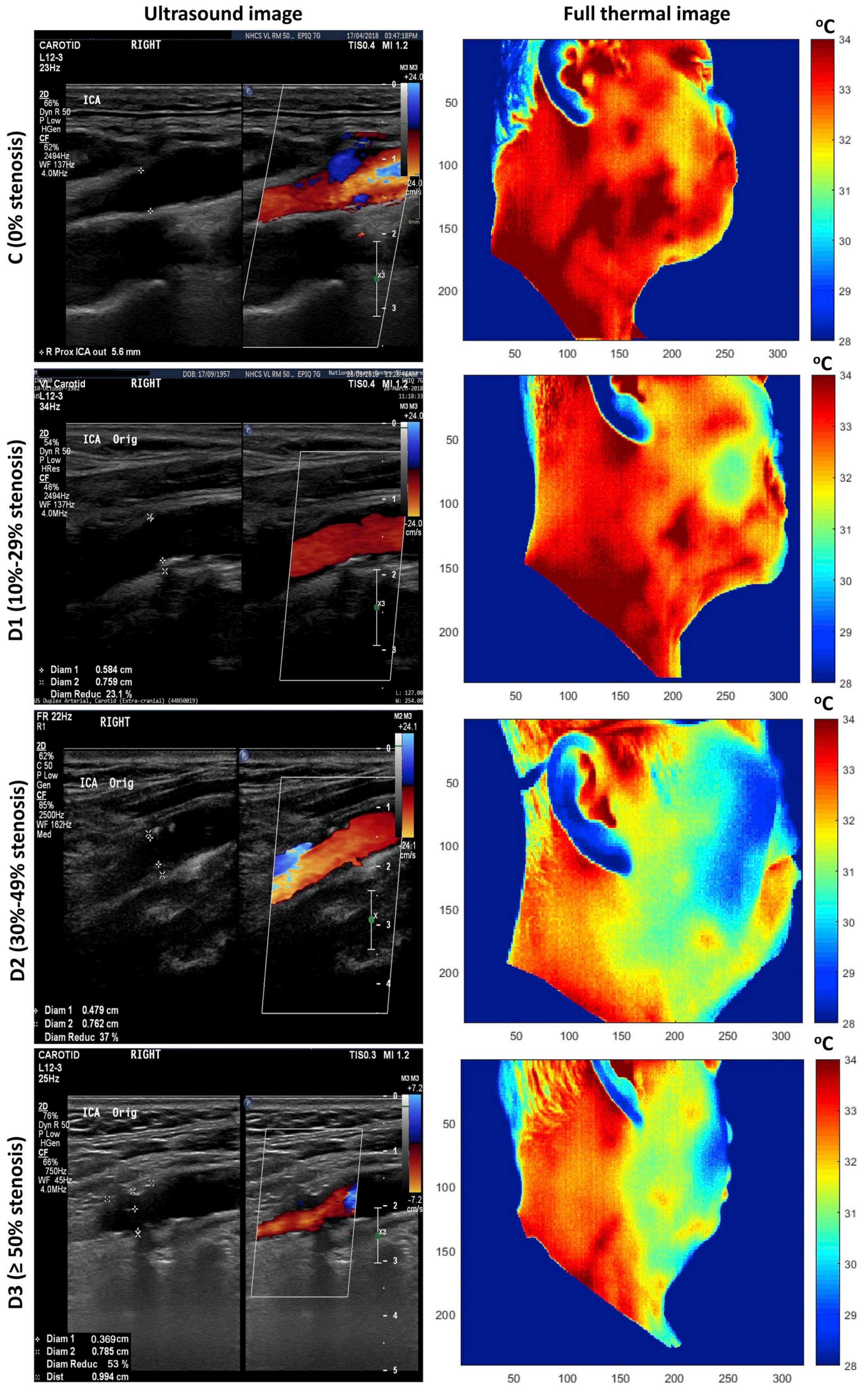

Fig. 4. Ultrasound image of the internal carotid artery section (ICA) and corresponding thermal image for a single patient from each of C, D1, D2 and D3 groups.

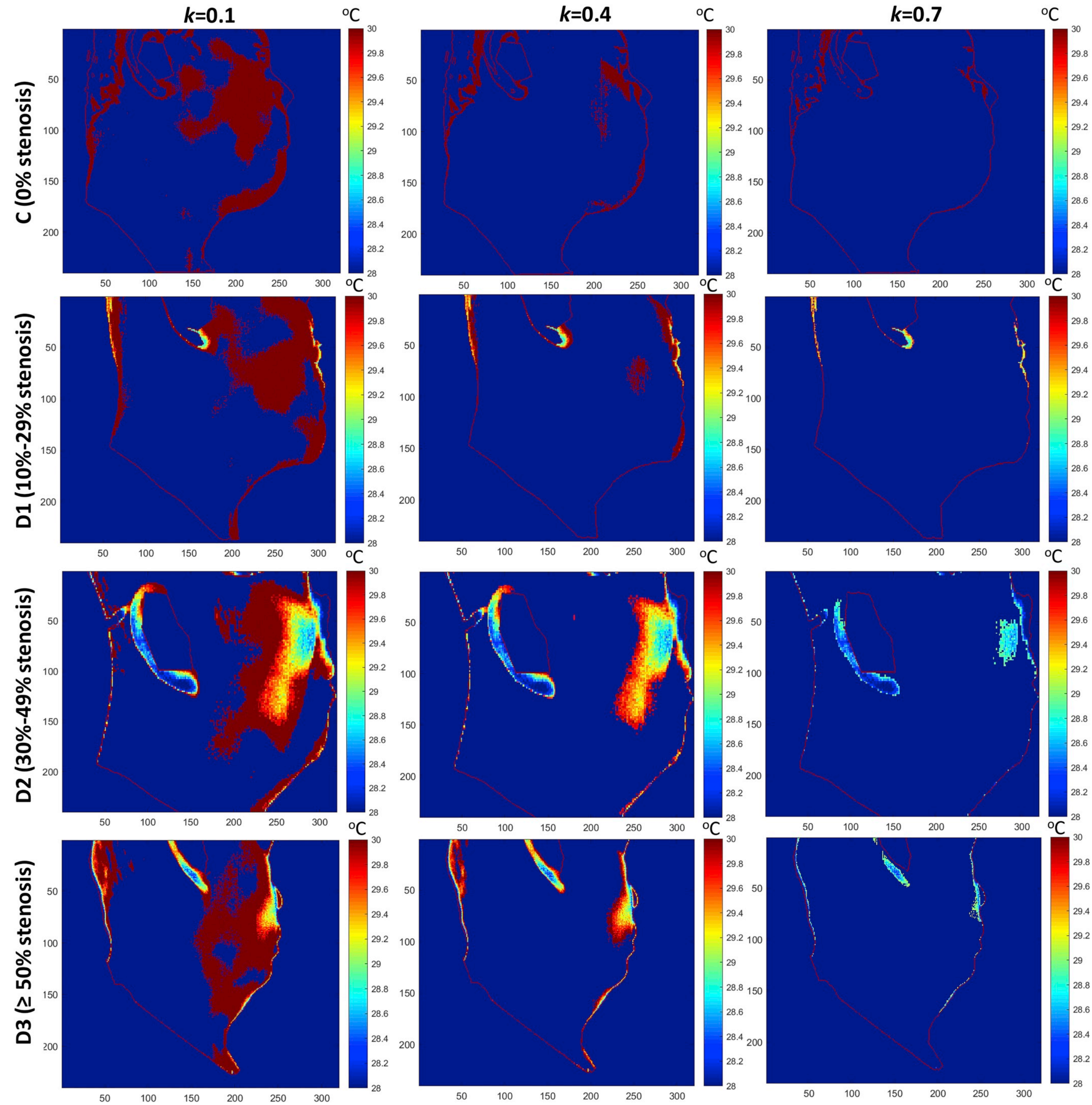

Fig. 5. Cold thermal feature image (at k = 0.1, 0.4, and 0.7) for a single patient from each of C, D1, D2 and D3 groups.

Table 2
Performance of the cut-off value-based binary classification model for various groups of patients using significant features from full thermal images.

Groups	Thermal feature cut-off value	Sensitivity (%)	Specificity (%)	AUC	Accuracy (%)	PPV (%)	NPV (%)
C′ and D′	Energy: 0.51	64	53	0.57	58	50	67
	Mean: 32.69	61	62	0.67	62	54	68
	Skewness: -0.42	79	62	0.68	69	60	80
	Kurtosis: 3.12	70	60	0.64	64	56	73
C and D1	Mean: 32.83	64	65	0.64	64	70	59
	Skewness: -0.45	56	75	0.68	64	74	58
D2 and D3	Skewness: -0.19	80	65	0.67	70	50	88

C: 0% stenosis; D1: 10%–29% stenosis; D2: 30%–49% stenosis; D3: ≥50% stenosis; C’: 0%–29% stenosis; D’: ≥30% stenosis; AUC: Area under the receiver operating characteristics (ROC) curve.

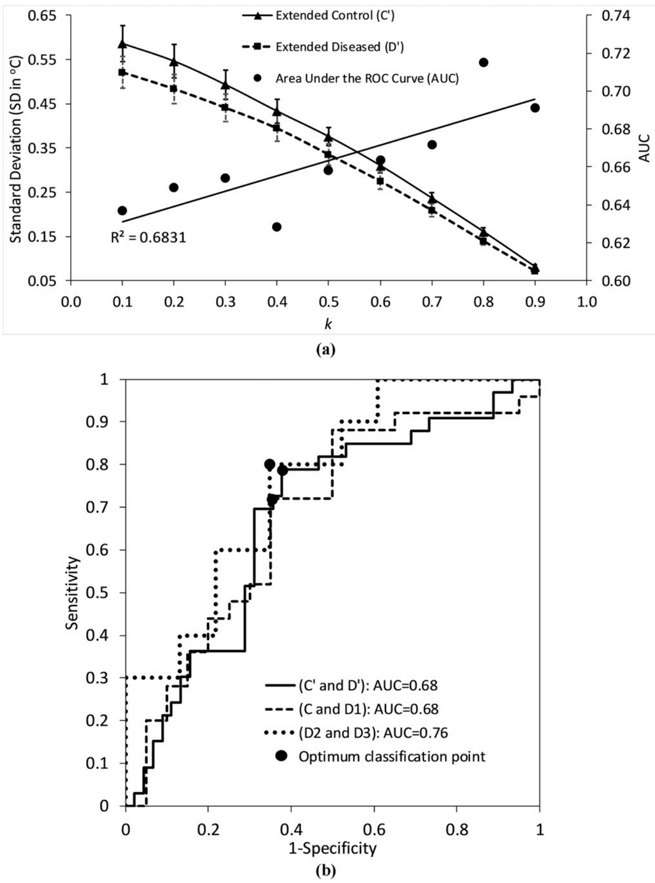

Fig. 6. (a) Standard deviation feature versus k for extended groups C′ and D′ and its binary classification performance in terms of area under the receiver operating characteristics (ROC) curve (AUC) (b) ROC curve to evaluate optimum classification cut-off value point for groups (C′ and D′), (C and D1), and (D2 and D3) for features skewness, contrast, and skewness, respectively, from full and cold thermal feature images.

in the supplementary material (Tables S1 and S2). For SD feature, the highest AUC value of 0.72, at $k = 0.8$ *cold thermal feature image*, resulted in a sensitivity and specificity of 73% and 63%, respectively. On the other hand, with slightly lower specificity, the skewness feature, extracted from the *full thermal image*, resulted in an improvement of 8% in the sensitivity of the classification (Table 3). In the sub-classification groups, (C and D1) and (D2 and D3), *cold thermal feature images* at $k = 0.2$ and 0.9, respectively, provided the highest classification performance (Table 3).

In contrast to the cut-off value-based binary classification model, the SVM-RBF model resulted in a better performance. Given that the SVM-RBF was tested using cross-validation, an average value (±95% CI) of the classification performance is reported in Table 4. For the extended group classification (C′ and D′), the sensitivity to classify patients with ≥30% stenosis in the carotid artery (D') was found to be 89%, which is 10% higher than the best cut-off value-based model. With an improvement of 56% from cut-off value model, the specificity of SVM-RBF model classification (classify patient with <30% stenosis) was found to be 97%. In the sub-classification groups, compared to the cut-off value model, while SVM-RBF model resulted in a substantial improvement in the sensitivity and specificity of classification in the group (C and D1), with a similar sensitivity of 80%, specificity improvement of 33% is observed in the group (D2 and D3) (Fig. 7). For all the three groups, while the cut-off value-based classification model resulted in an accuracy of around 70%, the accuracy of the SVM-RBF classification model was 92% or higher (Tables 3 and 4). Given that the SVM-RBF model has utilized all the significant features (Table 1) to perform the classification by mapping the features in a high-dimensional feature space, on the contrary to the cut-off value model, SVM-RBF model resulted in high classification performance. Though justified against the literature [40,47–49], the results of this study are limited by the number of samples. In the past studies on medical thermography-based disease diagnostic applications, utilizing cross-validation technique, high dimensional features extracted from small sample sizes of 50 (25 in each class) [30,34] and 90 (45 in each class) [24] were used to perform the SVM-based binary classification. Given the use of SVM model for thermography-based disease diagnostic applications in the past studies, to prove the potential of improving the classification performance from the cut-off value-based model for carotid stenosis detection [20], the present study is limited to the use of SVM-based machine learning model only. With the demonstrated high performance with the SVM model, this study paves the path for the future studies on the evaluation of the best machine learning-based classification model, along with the application of deep neural network-based classification [50–52].

5. Clinical outlook

Currently, there is no temperature-feature based non-invasive and non-contact carotid stenosis screening test available. The proposed thermography-based screening tool offers a fast and easy-to-use diagnostic. On average, a carotid ultrasound takes about 30 min that requires a trained sonographer to perform the examination and analyse the results thereafter [53]. With thermography, it takes only a few seconds to perform the examination once the patient is positioned appropriately. This time is, however, excluding the 15-min waiting time to bring the

Table 3
Performance of the cut-off value-based binary classification model for various groups of patients using significant features from full and cold thermal feature images.

Groups	*k*	Thermal feature cut-off value	Sensitivity (%)	Specificity (%)	AUC	Accuracy (%)	PPV (%)	NPV (%)
C′ and D′	Full thermal image	Skewness: -0.42	79	62	0.68	69	60	80
C and D1	0.2	Contrast: 1.54	72	65	0.68	69	72	65
D2 and D3	0.9	Skewness: -0.09	80	65	0.76	70	50	88

C: 0% stenosis; D1: 10%–29% stenosis; D2: 30%–49% stenosis; D3: ≥50% stenosis; C': 0%–29% stenosis; D': ≥30% stenosis; AUC: Area under the receiver operating characteristics (ROC) curve.

Table 4
Performance (±95% CI) of the SVM-RBF binary classification model for various groups of patients using all the significant features.

Groups	Number of features	Sensitivity (%)	Specificity (%)	Accuracy (%)	PPV (%)	NPV (%)
C′ and D′	19	89.4 ± 1.0	97.3 ± 0.9	94.1 ± 0.5	95.8 ± 1.3	93.0 ± 0.6
C and D1	14	96.4 ± 1.8	87.8 ± 1.9	92.6 ± 0.7	90.8 ± 1.2	95.3 ± 2.2
D2 and D3	5	80.3 ± 5.0	97.6 ± 1.5	92.7 ± 1.2	93.8 ± 3.9	92.7 ± 1.7

C: 0% stenosis; D1: 10%–29% stenosis; D2: 30%–49% stenosis; D3: ≥50% stenosis; C': 0%–29% stenosis; D': ≥30% stenosis.

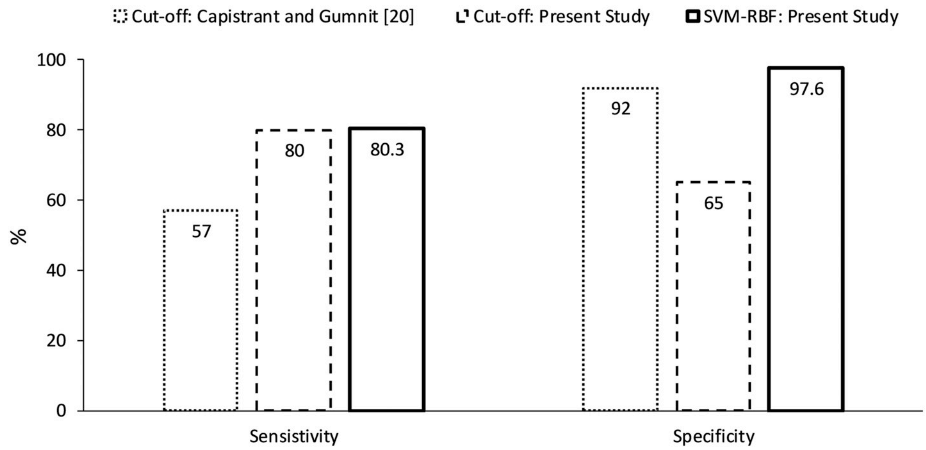

Fig. 7. Performance comparison to classify patients with ≥50% stenosis (D3).

body in thermal equilibrium with the ambient condition [54]. It should be noted that unlike a carotid ultrasound, the patient is not under examination for this 15-min waiting time. According to the MDsave cost estimation website [55], the cost of carotid ultrasound ranges from US $217 to US$700. Though the cost of the thermography-based examination is not estimated yet, intuitively, with no need for a bulky set-up, highly skilled operator, and reduced time of examination, it is expected to be a relatively low-cost examination [56]. Further, only the high-risk patients as detected by the proposed low-cost thermography-based screening shall be prescribed for further investigative diagnostics, hence, complementing the current clinical stenosis diagnosis. Relatively, such a screening examination will be more beneficial to the low and middle-income countries, where both the stroke-related deaths [57] and the patient to medical facilities ratio are high [58–60]. Other than the symptomatic carotid stenosis group of patients, given there is a possible relation between carotid stenosis and postoperative stroke incidences, carotid ultrasound scans are performed before the cardiac surgical procedures like coronary artery bypass grafting [61]. In a study on 295 patients undergoing by-pass surgery, only 72 were found to have significant stenosis [62]. Therefore, based on factors like female sex, peripheral vascular disease, history of transient ischemic attack or stroke, smoking, and coronary artery disease, correlations were explored to perform a preoperative carotid ultrasound on high risks patient only [63]. However, this adds to the cost and time burden on the overall treatment. In such a scenario, thermography could be an alternative carotid screening solution. Additionally, for asymptomatic patients, mass-screening for even high-risk patients (age, smoking, alcohol, diabetes, etc.) is not recommended. According to the Society of Vascular Surgery (SVS), screening all 60-year-old high-risk patients with DUS would cost £17 million (US$21 million). This will result in preventing about 230 strokes annually in the UK, which represents only 0.2% of the annual UK stroke burden [64]. Hence, the cost versus advantage is not justified. However, with the expected low-cost thermography-based screening tool, the cost versus advantage ratio may justify the implementation of such a mass screening.

6. Conclusions

In the present study, infrared (IR) thermography images were used to evaluate the presence of stenosis in the carotid artery. The intended patient classification study was performed on three classification groups, namely, (C': 0%–29% stenosis and D': ≥30% stenosis), (C: 0% stenosis and D1: 10%–29%), and (D2: 30%–49% and D3: ≥50% stenosis). From the background-subtracted original thermal image (referred to as *full thermal image*), using a novel parametric thermal feature extraction method, *cold thermal feature images* were extracted. Using the significant statistical features from both the *full* and *cold thermal feature images*, the binary classification problem was solved using the cut-off value and SVM-RBF classification models. With the demonstrated high sensitivity, specificity, and accuracy of the SVM-RBF classification model, this preliminary study suggests the potential of an IR thermography-based fast, non-contact, and non-invasive screening test for carotid artery stenosis disease. To generalize the findings, the demonstrated method needs to be tested in a large cohort clinical study, along with the use of a multi-class classification approach.

Conflicts of interest

The authors would like to declare that in addition to this work, they have a patent/copyright application on "Neck Thermography for a Non-contact/Non-invasive Screening of Patients with Carotid Artery Stenosis" at NTUitive Pte Ltd, Singapore.

Declaration of interests

The authors declare the following financial interests/personal relationships which may be considered as potential competing interests: The authors would like to declare that in addition to this work, they have a patent/copyright application on "Neck Thermography for a Non-contact/Non-invasive Screening of Patients with Carotid Artery Stenosis" at NTUitive Pte Ltd, Singapore.

Acknowledgement

The authors acknowledge the SingHealth-NTU collaborative research grant (Grant number: SHS-NTU/014/2016) for the funding support to carry out this project. The authors would also like to acknowledge their heartfelt gratitude to the staff of vascular lab (NHCS: National Heart Center Singapore), Ms. Siti Aishah Binte Mohd Hassan (NHCS), Mr. Vignesh Raman (former research staff, NTU), and Eetarp Engineering Pte. Ltd., Singapore, for the carotid artery duplex ultrasound data collection, patient recruitment assistance, thermography data collection, and providing the infrared (IR) thermal camera support, respectively.

Appendix A. Supplementary data

Supplementary data to this article can be found online at https://doi.org/10.1016/j.compbiomed.2019.103419.

References

[1] J. Sanz, Z. a Fayad, Imaging of atherosclerotic cardiovascular disease, Nature 451 (2008) 953–957, https://doi.org/10.1038/nature06803.

[2] A.S. Jahromi, C.M. Clase, R. Maggisano, R. Bailey, H.A. Safar, C.S. Cinà, Progression of internal carotid artery stenosis in patients with peripheral arterial occlusive disease, J. Vasc. Surg. 50 (2009) 292–298, https://doi.org/10.1016/j.jvs.2009.02.236.

[3] E.J. Benjamin, P. Muntner, A. Alonso, M.S. Bittencourt, C.W. Callaway, A. P. Carson, A.M. Chamberlain, A.R. Chang, S. Cheng, S.R. Das, F.N. Delling, L. Djousse, M.S.V. Elkind, J.F. Ferguson, M. Fornage, L.C. Jordan, S.S. Khan, B. M. Kissela, K.L. Knutson, T.W. Kwan, D.T. Lackland, T.T. Lewis, J.H. Lichtman, C. T. Longenecker, M.S. Loop, P.L. Lutsey, S.S. Martin, K. Matsushita, A.E. Moran, M. E. Mussolino, M. O'Flaherty, A. Pandey, A.M. Perak, W.D. Rosamond, G.A. Roth, U. K.A. Sampson, G.M. Satou, E.B. Schroeder, S.H. Shah, N.L. Spartano, A. Stokes, D. L. Tirschwell, C.W. Tsao, M.P. Turakhia, L.B. VanWagner, J.T. Wilkins, S.S. Wong, S.S. Virani, Heart disease and stroke statistics—2019 update: a report from the American heart association, Circulation 139 (2019) e56–e528, https://doi.org/10.1161/cir.0000000000000659.

[4] J.J. Ricotta, J. Pagan, M. Xenos, Y. Alemu, S. Einav, D. Bluestein, Cardiovascular disease management: the need for better diagnostics, Med. Biol. Eng. Comput. 46 (2008) 1059–1068, https://doi.org/10.1007/s11517-008-0416-x.

[5] A. Saxena, E.Y.K. Ng, S.T. Lim, Imaging modalities to diagnose carotid artery stenosis: progress and prospect, Biomed. Eng. Online 18 (2019) 1–23, https://doi.org/10.1186/s12938-019-0685-7.

[6] T. Kohler, Y. Langlois, G.O. Roederer, D.J. Phillips, K.W. Beach, J. Primozich, R. Lawrence, S.C. Nicholls, D.E. Strandness, Sources of variability in carotid duplex examination: a prospective study, Ultrasound Med. Biol. 11 (1985) 571–576, https://doi.org/10.1016/0301-5629(85)90027-4.

[7] W.-C. Lan, Y.-H. Chen, S.-H. Liu, Non-invasive imaging modalities for the diagnosis of coronary artery disease: the present and the future, Tzu Chi Med. J. 25 (2013) 206–212, https://doi.org/10.1016/j.tcmj.2013.04.004.

[8] M.R. Angiography (MRA), RadiologyInfo.Org.. https://www.radiologyinfo.org/en/info.cfm?pg=angiomr, 2019. (Accessed 27 August 2019).

[9] Information for Consumers, Magnetic resonance Angiography (MRA), Dep. Heal. West. Aust. (2017), in: http://www.imagingpathways.health.wa.gov.au/index.php/consumer-info/imaging-procedures/magnetic-resonance-angiography-mra. (Accessed 27 August 2019).

[10] T. Dowsley, M. Al-Mallah, K. Ananthasubramaniam, G. Dwivedi, B. McArdle, B.J. W. Chow, The role of noninvasive imaging in coronary artery disease detection, Prognosis, and clinical decision making, Can. J. Cardiol. 29 (2013) 285–296, https://doi.org/10.1016/j.cjca.2012.10.022.

[11] A. Huibers, G.J. De Borst, S. Wan, F. Kennedy, A. Giannopoulos, F.L. Moll, T. Richards, Non-invasive carotid artery imaging to identify the vulnerable plaque: current status and future goals, Eur. J. Vasc. Endovasc. Surg. 50 (2015) 563–572, https://doi.org/10.1016/j.ejvs.2015.06.113.

[12] X. Huang, C. Yang, C. Yuan, F. Liu, G. Canton, J. Zheng, K. Woodard, G.A. Sicard, D. Tang, Patient-specific artery shrinkage and 3D zero-stress state in multi-component 3D FSI models for carotid atherosclerotic plaques based on in-vivo MRI data, Mol. Cell. Biomech. 6 (2009) 121–134.

[13] M.L. Ong, E.Y.K. Ng, A global bioheat model with self-tuning optimal regulation of body temperature using Hebbian feedback covariance learning, Med. Phys. 32 (2005) 3819–3831, https://doi.org/10.1118/1.2133720.

[14] Y. Yang, J. Liu, Detection of atherosclerosis through mapping skin temperature variation caused by carotid atherosclerosis plaques, J. Therm. Sci. Eng. Appl. 3 (2011) 1–9, https://doi.org/10.1115/1.4004109.

[15] A. Saxena, E.Y.K. Ng, M. Mathur, C. Manchanda, N.A. Jajal, Effect of carotid artery stenosis on neck skin tissue heat transfer, Int. J. Therm. Sci. 145 (2019), https://doi.org/10.1016/j.ijthermalsci.2019.106010.

[16] B. Hofferberth, M. Gottschaldt, S. Dykan, Comparison of Doppler sonography and plate thermography for detection of carotid artery stenosis, Stroke 11 (1980) 27–30, https://doi.org/10.1161/01.STR.11.1.27.

[17] A. Saxena, V. Raman, E.Y.K. Ng, Study on methods to extract high contrast image in active dynamic thermography, Quant. InfraRed Thermogr. J. 6733 (2019) 1–17, https://doi.org/10.1080/17686733.2019.1586376.

[18] A. Saxena, E.Y.K. Ng, V. Raman, Thermographic venous blood flow characterization with external cooling stimulation, Infrared Phys. Technol. 90 (2018) 8–19, https://doi.org/10.1016/j.infrared.2018.02.001.

[19] A. Saxena, V. Raman, E.Y.K. Ng, Single image reconstruction in active dynamic thermography: a novel approach, Infrared Phys. Technol. 93 (2018) 53–58, https://doi.org/10.1016/j.infrared.2018.07.020.

[20] T.D. Capistrant, R.J. Gumnit, Detecting carotid occlusive disease by thermography, Stroke 4 (1973) 57–64.

[21] J. Thiruvengadam, M. Anburajan, M. Menaka, B. Venkatraman, Potential of thermal imaging as a tool for prediction of cardiovascular disease, J. Med. Phys. 39 (2014) 98–105, https://doi.org/10.4103/0971.

[22] P.B. Morgan, J.V. Smyth, A.B. Tullo, N. Efron, Ocular temperature in carotid artery stenosis, Optom. Vis. Sci. 76 (1999) 850–854.

[23] G. Von Reutern, M. Goertler, N.M. Bornstein, F. Perren, A. Razumovky, T. Shiogai, Grading carotid stenosis using ultrasonic methods, Stroke (2012) 916–921, https://doi.org/10.1161/STROKEAHA.111.636084.

[24] F. Dong, C. Tao, J. Wu, Y. Su, Y. Wang, Y. Wang, Detection of cervical lymph node metastasis from oral cavity cancer using a non-radiating , noninvasive digital infrared thermal imaging system, Sci. Rep. (2018) 1–9, https://doi.org/10.1038/s41598-018-24195-4.

[25] P. Hung, K. Lee, L. Tsai, Contact-free heart rate measurement using multiple video data, in: AIP Conf. Proc., 2013, pp. 57–66, https://doi.org/10.1063/1.4824996.

[26] N. Sun, M. Garbey, A. Merla, I. Pavlidis, Imaging the cardiovascular pulse, Proc IEEE Comput. Soc. Conf. Comput. Vis. Pattern Recognit. 2 (2005) 416–421, https://doi.org/10.1109/CVPR.2005.184.

[27] S. Kacmaz, E. Ercelebi, S. Zengin, S. Cindoruk, The use of infrared thermal imaging in the diagnosis of deep vein thrombosis, Infrared Phys. Technol. 86 (2017) 120–129, https://doi.org/10.1016/j.infrared.2017.09.005.

[28] N.R. Pal, S.K. Pal, A review on image segmentation techniques, Pattern Recognit. 26 (1993).

[29] E.F.J. Ring, K. Ammer, Infrared thermal imaging in medicine, Physiol. Meas. Top. 33 (2012) R33–R46, https://doi.org/10.1088/0967-3334/33/3/R33.

[30] U.R. Acharya, E.Y.K. Ng, J. Tan, Thermography based breast cancer detection using texture features and support vector machine, J. Med. Syst. 36 (2012) 1503–1510, https://doi.org/10.1007/s10916-010-9611-z.

[31] L.I.B. Onanno, S.I.M. Arino, P.L.B. Ramanti, F.A.S. Ottile, Validation of a computer-aided diagnosis system for the automatic identification of carotid atherosclerosis, Ultrasound Med. Biol. 41 (2019) 509–516, https://doi.org/10.1016/j.ultrasmedbio.2014.09.004.

[32] T. Fawcett, An introduction to ROC analysis, Pattern Recognit. Lett. 27 (2006) 861–874, https://doi.org/10.1016/j.patrec.2005.10.010.

[33] Víctor Martínez-Cagigal, ROC curve. https://www.mathworks.com/matlabcentral/fileexchange/52442-roc-curve, 2019.

[34] U. Raghavendra, U.R. Acharya, E.Y.K. Ng, J. Tan, An integrated index for breast cancer identification using histogram of oriented gradient and kernel locality preserving projection features extracted from thermograms, Quant. InfraRed Thermogr. J. 13 (2016) 195–209, https://doi.org/10.1080/17686733.2016.1176734.

[35] H. Madhu, S.T. Kakileti, K. Venkataramani, S. Jabbireddy, Extraction of medically interpretable features for classification of malignancy in breast thermography, in: 2016 38th Annu. Int. Conf. IEEE Eng. Med. Biol. Soc., 2016, pp. 1062–1065.

[36] C. Jin, Z. Xue, K. Liu, Automated analysis method for screening knee osteoarthritis using medical infrared thermography, J. Med. Biol. Eng. 33 (2013) 471–477, https://doi.org/10.5405/jmbe.1054.

[37] K.-R. Müller, S. Mika, G. Rätsch, K. Tsuda, B. Schölkopf, An introduction to kernel-based learning algorithms, IEEE Trans. Neural Netw. 12 (2001) 181–201.

[38] A. Ng, Support vector machines, in: CS229 Lect. Notes, 2000, pp. 1–25.

[39] Y. Jung, J. Hu, A K-fold averaging cross-validation procedure, J. Nonparametric Statistics 27 (2015) 167–179, https://doi.org/10.1080/10485252.2015.1010532.

[40] R. Devi, H.K. Tyagi, D. Kumar, A novel multi-class approach for early-stage prediction of sudden cardiac death, Biocybern. Biomed. Eng. 39 (2019) 586–598, https://doi.org/10.1016/j.bbe.2019.05.011.

[41] M. Szczerbo-trojanowska, T. Jargie, A. Drelich-zbroja, Management of carotid stenosis: history and today, J. Ultrason. 13 (2013) 6–20.

[42] M. Öner, İ. Deveci Kocakoç, Jmasm 49: a compilation of some Popular goodness of fit tests for normal distribution: their algorithms and MATLAB codes (MATLAB), J. Mod. Appl. Stat. Methods 16 (2017) 547–575, https://doi.org/10.22237/jmasm/1509496200.

[43] J.D. Gibbons, S. Chakraborti, Nonparametric Statistical Inference, fourth ed., Marcel Dekker, Inc., New York, USA, 1992. http://www.amazon.com/Nonparametric-Statistical-Inference-Statistics-Monographs/dp/0824786610.

[44] R. Mittal, S.P. Simmons, F. Najjar, Numerical study of pulsatile flow in a constricted channel, J. Fluid Mech. 485 (2003) 337–378, https://doi.org/10.1017/S002211200300449X.

[45] S.A. Urquiza, P.J. Blanco, Multidimensional modelling for the carotid artery blood flow, Comput. Methods Appl. Mech. Eng. 195 (2006) 4002–4017, https://doi.org/10.1016/j.cma.2005.07.014.

[46] A. Saxena, E.Y.K. Ng, Steady and Pulsating flow past a heated rectangular cylinder (s) in a channel, J. Thermophys. Heat Transf. 8722 (2017) 1–13, https://doi.org/10.2514/1.T5265.

[47] S. Mukherjee, P. Tamayo, S. Rogers, R. Rifkin, A. Engle, C. Campbell, T.R. Golub, J. P. Mesirov, Estimating Dataset size requirements for classifying DNA microarray data, J. Comput. Biol. 10 (2003) 119–142, https://doi.org/10.1089/106652703321825928.

[48] K. Hajian-Tilaki, Sample size estimation in diagnostic test studies of biomedical informatics, J. Biomed. Inform. 48 (2014) 193–204, https://doi.org/10.1016/j.jbi.2014.02.013.

[49] Y. Yu, T. McKelvey, S.Y. Kung, A classification scheme for high-dimensional-small-sample-size data using soda and ridge-SVM with microwave measurement applications, in: ICASSP, IEEE Int. Conf. Acoust. Speech Signal Process. - Proc., IEEE, 2013, pp. 3542–3546, https://doi.org/10.1109/ICASSP.2013.6638317.

[50] S. Xie, T. Yang, X. Wang, Y. Lin, Hyper-class augmented and regularized deep learning for fine-grained image classification, in: Proc. IEEE Comput. Soc. Conf. Comput. Vis. Pattern Recognit., IEEE, 2015, pp. 2645–2654, https://doi.org/10.1109/CVPR.2015.7298880.

[51] O. Yildirim, M. Talo, B. Ay, U.B. Baloglu, G. Aydin, U.R. Acharya, Automated detection of diabetic subject using pre-trained 2D-CNN models with frequency spectrum images extracted from heart rate signals, Comput. Biol. Med. 113 (2019) 103387, https://doi.org/10.1016/j.compbiomed.2019.103387.

[52] Y. Liu, J.W. Bi, Z.P. Fan, Multi-class sentiment classification: the experimental comparisons of feature selection and machine learning algorithms, Expert Syst. Appl. 80 (2017) 323–339, https://doi.org/10.1016/j.eswa.2017.03.042.

[53] Carotid ultrasound, mayo clin (n.d.), https://www.mayoclinic.org/tests-procedures/carotid-ultrasound/about/pac-20393399. (Accessed 24 July 2019).

[54] I. Fernández-Cuevas, J.C. Bouzas Marins, J. Arnáiz Lastras, P.M. Gómez Carmona, S. Piñonosa Cano, M.Á. García-Concepción, M. Sillero-Quintana, Classification of factors influencing the use of infrared thermography in humans: a review, Infrared Phys. Technol. 71 (2015) 28–55, https://doi.org/10.1016/j.infrared.2015.02.007.

[55] MDsave, Carotid ultrasound/Doppler (n.d.), https://www.mdsave.com/procedures/carotid-ultrasound-doppler/d783feca. (Accessed 24 July 2019).

[56] N. Arora, D. Martins, D. Ruggerio, E. Tousimis, A.J. Swistel, M.P. Osborne, R. M. Simmons, Effectiveness of a noninvasive digital infrared thermal imaging system in the detection of breast cancer, Am. J. Surg. 196 (2008) 523–526, https://doi.org/10.1016/j.amjsurg.2008.06.015.
[57] Cardiovascular diseases (CVDs), World heal. Organ (n.d.), https://www.who.int/en/news-room/fact-sheets/detail/cardiovascular-diseases-(cvds. (Accessed 24 July 2019).
[58] D.O. Abegunde, C.D. Mathers, T. Adam, M. Ortegon, K. Strong, The burden and costs of chronic diseases in low-income and middle-income countries, Lancet 370 (2007) 1929–1938, https://doi.org/10.1016/S0140-6736(07)61696-1.
[59] S. Bagcchi, India has low doctor to patient ratio, study finds, BMJ 351 (2015) h5195, https://doi.org/10.1136/bmj.h5195.
[60] D.H. Peters, A. Garg, G. Bloom, D.G. Walker, W.R. Brieger, M. Hafizur Rahman, Poverty and access to health care in developing countries, Ann. N. Y. Acad. Sci. 1136 (2008) 161–171, https://doi.org/10.1196/annals.1425.011.
[61] K. Masabni, S. Raza, E.H. Blackstone, H.L. Gornik, J.F. Sabik III, Does preoperative carotid stenosis screening reduce perioperative stroke in patients undergoing coronary artery bypass grafting? Ournal Thorac. Cardiovasc. Surg. 149 (2015) 1253–1260, https://doi.org/10.1016/j.jtcvs.2015.02.003.
[62] R.G. Sheiman, B.J. D'Othée, Screening carotid sonography before elective coronary artery bypass graft surgery: who needs it, Am. J. Roentgenol. 188 (2007) 475–479, https://doi.org/10.2214/AJR.06.1024.
[63] D.C. Silver, E.S. Berens, N.T. Kouchoukos, S.F. Murphy, Preoperative carotid artery screening in elderly patients undergoing cardiac surgery, J. Vasc. Surg. 15 (1992) 0313–0323, https://doi.org/10.1067/mva.1992.33806.
[64] C.D. Liapis, Editor's choice - management of atherosclerotic carotid and vertebral artery disease: 2017 clinical Practice guidelines of the european society for vascular surgery (ESVS), Eur. J. Vasc. Endovasc. Surg. 55 (2018) 3–81, https://doi.org/10.1016/j.ejvs.2018.03.022.

Ashish Saxena: Ashish is a full-time Ph.D. student at Nanyang Technological University, Singapore. He is currently working on the development of passive and active thermographic methods (tools/device) to perform patient screening for cardiovascular-related diseases. With a mechanical and thermal engineering background, his research interests include studying hemodynamics influenced tissue heat transfer using computational fluid dynamics methods, thermography-based sensing and imaging, biomedical diagnostic/clinical research, and thermo-regulation of solar photovoltaics.

Eddie Yin Kwee Ng: Ng, currently serving as an Associate Professor at Nanyang Technological University, Singapore, has obtained his Ph.D from Cambridge University. He is the Editor-in-Chief for the ISI Journal of Mechanics in Medicine and Biology and the Founding Editor-in-Chief for the ISI indexed Journal of Medical Imaging and Health Informatics. His main area of research is human physiology, biomedical engineering, computational fluid dynamics and numerical heat transfer.

Lim Soo Teik: Lim is Deputy Medical Director, National Heart Centre Singapore (NHCS), and Director of the Cardiac Catheterization Laboratory and Senior Consultant with the Department of Cardiology at NHCS. He is also the Deputy Academic vice-Chair, Training & Education in the Cardiovascular Sciences Academic Clinical Program. Lim's subspecialty interest is in interventional cardiology. He is specialized in coronary angioplasty and stenting, as well as peripheral vascular interventional treatment for diseases in carotid, renal, iliac and lower limb vessels. Additionally, he has a special interest in the management of pulmonary hypertension, dyslipidemia and hypertension.